Smart Structures and Systems, *Vol. 23, No. 3 (2019) 227-242*
DOI: https://doi.org/10.12989/sss.2019.23.3.227

Probabilistic behavior of semi-active isolated buildings under pulse-like earthquakes

Seda Öncü-Davas[a] and Cenk Alhan[*]

Department of Civil Engineering, Istanbul University-Cerrahpaşa, Turkey

(Received October 30, 2018, Revised February 16, 2019, Accepted February 20, 2019)

Abstract. Seismic isolation systems employ structural control that protect both buildings and vibration-sensitive contents from destructive effects of earthquakes. Structural control is divided into three main groups: passive, active, and semi-active. Among them, semi-active isolation systems, which can reduce floor displacements and accelerations concurrently, has gained importance in recent years since they don't require large power or pose stability problems like active ones. However, their seismic performance may vary depending on the variations that may be observed in the mechanical properties of semi-active devices and/or seismic isolators. Uncertainties relating to isolators can arise from variations in geometry, boundary conditions, material behavior, or temperature, or aging whereas those relating to semi-active control devices can be due to thermal changes, inefficiencies in calibrations, manufacturing errors, etc. For a more realistic evaluation of the seismic behavior of semi-active isolated buildings, such uncertainties must be taken into account. Here, the probabilistic behavior of semi-active isolated buildings under historical pulse-like near-fault earthquakes is evaluated in terms of their performance in preserving structural integrity and protecting vibration-sensitive contents considering aforementioned uncertainties via Monte-Carlo simulations of 3-story and 9-story semi-active isolated benchmark buildings. The results are presented in the form of fragility curves and probability of failure profiles.

Keywords: semi-active isolation; probabilistic behavior; historical pulse-like earthquakes; uncertainty; fragility curve

1. Introduction

When serious dynamic effects of earthquakes on structures are of concern, ensuring the safety of the people, prevention of structural and non-structural damage, and the protection of vibration-sensitive equipment housed in the special-purpose structures are crucial priorities. Therefore, the use of seismic isolation systems that employ semi-active structural control, which offers high seismic performance, is gaining preference especially in the design of special-purpose structures. Structural control systems are dynamic systems in which properties such as stiffness or damping can be adjusted online so that the dynamic response parameters of the structure (acceleration, displacement, etc.) do not exceed acceptable levels (Cheng *et al.* 2008). On the other hand, passive systems can be used effectively to protect the buildings from a specific dynamic load, but their effectiveness may be low for other dynamic load types (Saaed *et al.* 2015). Passive seismic isolation systems are being questioned for more than two decades because of the high damping needs to reduce large base displacements which may occur under near-fault earthquakes involving long period and high amplitude velocity pulses as they can be less successful under moderate far-fault earthquakes when they are designed with high passive damping for such severe near-fault earthquakes (Johnson *et al.* 1998). High damping may lead to amplifications both in the floor accelerations and inter-story drift ratios. While amplifications in floor accelerations may be critical for vibration-sensitive equipment (Alhan and Şahin 2011, Alhan and Öncü-Davas 2016, Providakis 2009), amplifications in inter-story drift ratios may threaten the integrity and thus the safety of the whole structural system as well as non-structural elements such as partitions, walls, etc. (Gavin and Alhan 2004, Providakis 2008). Gavin and Alhan (2004) showed that increasing damping may lead to increase in inter-story drifts. Providakis (2008) pointed out that the isolated buildings with high (additional) damping are susceptible to damage if the inter-story drifts are not carefully controlled. Due to these shortcomings, the research and development on semi-active isolation systems, which may offer a solution for such problems, have received remarkable attention in recent years.

Semi-active control systems are control systems that use devices whose mechanical properties such as damping and rigidity can be modified online. The semi-active control systems provide the adaptability of the active control systems and the reliability of the passive control systems (Saaed *et al.* 2015). Furthermore, unlike active control systems, these systems consume as little energy as a battery power and do not cause stability problems. Deterministic studies on semi-active isolation systems (Symans *et al.* 2000, Madden *et al.* 2003, Alhan *et al.* 2006) showed that these systems are effective in limiting base displacement without significantly increasing floor accelerations. Having said that, a realistic evaluation of the seismic performance

*Corresponding author, Professor
E-mail: cenkalhan@istanbul.edu.tr
[a] Ph.D.

 ISSN: 1738-1584 (Print), 1738-1991 (Online)

of semi-active isolation systems can only be possible by using a realistic mathematical model that takes uncertainties inherent in the isolation systems into account appropriately.

The uncertainties in the mechanical parameters of isolators can occur due to variations in the geometry, the boundary conditions, the constitutive behavior of materials (Chaudhuri and Chakraborty 2006), temperature changes and aging, (Shenton III and Holloway, 2000), and relative humidity and localized damage (Aly 2014). Similarly, uncertainties in semi-active control devices are related to their non-linear nature, thermal variations, poor calibration, or their malfunctioning (YeganehFallah and Taghikhany 2014). Roy *et al*. (2014) stressed that the uncertainties with regard to the system parameters and the stochastic nature of earthquake may lead to deviations in the structural response parameters from their deterministic values. Furthermore, these uncertainties can affect the structural reliability (Chaudhuri and Chakraborty 2006). Such uncertainties can be taken into account by probabilistic seismic risk and reliability analyses. And Monte-Carlo Simulation Technique is a suitable method for performing such analyses of complex engineering systems (Haldar and Mahadevan 2000) which was used in earlier studies related to the probabilistic analyses of seismically isolated buildings (Shenton III and Holloway 2000, Alhan and Gavin 2005, Perotti *et al*. 2013, Bakhshi and Mostafavi 2014). Other recent seismic risk studies related to different types of *passive* isolation systems in the literature include those conducted by (Alhan and Gavin 2005, Colombo and Almazan 2015, Chakraborty and Debbarma 2016, Saha *et al.* 2016, Castaldo *et al.* 2017, Tajammolian *et al*. 2018).

Although considerable probabilistic studies are conducted on passive seismic isolation systems as partly listed above, there exist only a few probabilistic studies on semi-active isolated buildings despite the increasing interest on the semi-active control systems in recent years. Chase *et al.* (2004) compared the impact of a type of semi-active control strategy on the structural responses and evaluated the results in terms of statistical distributions. Gavin and Zaicenco (2007) evaluated the reliability of passive and semi-active equipment isolation under historical earthquakes considering the uncertainties in the isolation system. Aly and Christenson (2008) proposed an energy-based probabilistic approach for evaluating the efficacy of smart damping technology. (Fallah and Taghikhany 2014) assessed the performance of robust semi-active control via numerical simulations. Three-story benchmark structure equipped with a single magneto-rheological damper is used in the simulations by taking into account the uncertainties of the structural model and the damper force. YeganehFallah and Attari (2017) proposed a robust controller for mitigating undesired uncertainty effects on the structural response of a cable-stayed bridge equipped with magneto-rheological dampers under historical earthquakes. Öncü-Davas and Alhan (2019) assessed the reliabilities of benchmark semi-active isolated buildings under synthetically developed near-fault pulses with no high-frequency content.

In the scope of this study, the probabilistic behavior of semi-active isolated buildings under historical pulse-like earthquakes are evaluated in terms of both protecting the vibration-sensitive equipment and preserving the structural integrity by taking into account the uncertainties in the mechanical parameters of the semi-active isolation system elements including the post-yield to pre-yield stiffness ratio, the yield displacement, and the yield force of the isolators and stiffness and damping of the semi-active control devices. A large number of historical pulse-like earthquake records is selected and divided into two groups according to the closest distances to the fault line (0-6 km and 6-10 km). 3 and 9-story benchmark semi-active isolated buildings are used in order to also take the influence of the superstructure flexibility on the reliability results into account. Examining structures with different number of floors is necessary since both the floor accelerations and the inter-story drift ratios can reach higher levels in the upper floors. Monte-Carlo simulations are conducted by performing non-linear time-history analyses for the determined number of simulations for each historical earthquake record via 3DBASIS-SA-MC which is a further modified version of 3DBASIS-SA (Gavin *et al.* 2003) which itself is a previously modified version of 3DBASIS program (Nagarajaiah *et al.* 1991). 3DBASIS-SA-MC (Öncü-Davas 2018) has the capability of carrying out recursive non-linear time history analyses of semi-actively isolated buildings which serves as a convenient tool for a Monte Carlo study. The results of this investigation are presented in the form of fragility curves and the probability of failure profiles along the height of the buildings.

2. Probabilistic analysis of semi-active buildings

If there is a possibility that there is more than one result of a problem, then the existence of uncertainties in that problem can be mentioned. Probabilistic analysis is performed for solving problems with uncertainties. In order to determine the reliability or the probability of failure, various probabilistic analysis methods such as first-order reliability methods (FORM), second-order reliability methods (SORM), or Monte-Carlo Simulation (MC) can be used (Haldar and Mahadevan 2000). Although results obtained by FORM method may be relatively accurate in non-complex practical design problems, it can lead to inaccurate results for high-order nonlinear problems and thus unreliable designs. It may be more appropriate to use the Monte-Carlo simulation method in highly nonlinear problems (Padmanabhan *et al.* 2006) as it gives more accurate results than SORM and FORM methods in solving such problems (Der Kiureghian 2000). For this reason, the Monte-Carlo simulation is preferred in this study for performing the probabilistic analyses of the buildings with semi-active isolation systems.

2.1 Monte-Carlo simulation technique

Monte-Carlo (MC) simulation technique is an accurate, robust and simple method for performing reliability analysis (Pradlwarter *et al.* 1998, Papaioannou *et al.* 2013). The stages to be performed for the MC simulation are as follows

(Haldar and Mahadevan 2000, Ayyub and Klir 2006):

i. Definition of random variables (i.e. parameters with uncertainties);

ii. Determination of probability distributions of random variables that are compatible with their nature;

iii. Generation of random numbers and calculation of random variables;

iv. Obtaining deterministic solution of the problem for each of the total number of simulations (n_{mc});

v. Statistical evaluation of the results;

vi. Investigation of the accuracy and the efficiency of the simulations so that the optimum number of simulations (nmc) is determined.

Fig. 1 schematically illustrates the Monte-Carlo Simulation (Sinha *et al.* 2013). Herein, firstly, random variables are determined (X_1, X_2 and X_n). Then, the random variables are distributed around the nominal values by generating random numbers equal to the total number of simulations (n_{mc}) with probability distribution functions such as normal, lognormal, uniform, Weibull, or exponential, etc. that are compatible with their nature. Note that, the probability density function (PDF) and the cumulative distribution function (CDF) are used to mathematically express the distributions. Finally, deterministic analyses are performed as many as the total number of simulations (nmc). Then, the results (R_1 and R_2) are processed and presented in a probabilistic manner.

2.2 Semi-active isolation system modeling

Semi-active control systems employ devices with mechanical components that operate with small energies such as a valve or a bolt friction connection. Semi-active control systems can be used in the superstructure or as an additional damping element in passive seismic isolation systems. In this study, a semi-active isolation system has been formed by using semi-active control devices in parallel with an isolation system that consists of rubber isolators. The force-displacement behavior of these isolators can be modeled as smooth bi-linear hysteretic (Nagarajaiah *et al.* 1991). Main relationships between the main mechanical parameters of the rubber isolators are tabulated in Table 1.

The nominal isolation periods (rigid-body periods) of the benchmark buildings used in this study are obtained via Eq. (1) depending on the total weight of the buildings (W) and the nominal total post-yield stiffness (K_{2t}) of the isolation system. Here, g is the gravitational acceleration and the post-yield stiffness per isolator can be obtained by dividing K_{2t} to the total number of isolators in the isolation systems. The pre-yield stiffness, K_1, the yield force, F_y, and the post-yield to pre-yield stiffness ratio, α, then can be can be obtained through the relationships given in Eqs. (2)-(4), respectively.

The other main component of a semi-active isolation system is the semi-active control device, which is basically a Maxwell visco-elastic element with a controllable damping coefficient (Gavin *et al.* 2003). Here, the semi-active Maxwell element is modeled as a spring element connected in series with a controllable damper element.

Table 1 Relationships between the main mechanical parameters of the rubber isolators

Equation	Mechanical parameter	Formulation
(1)	Nominal isolation period	$T_0 = 2\pi\sqrt{W/gK_{2t}}$
(2)	Characteristic force	$Q = (K_1\text{-}K_2)D_y$
(3)	Yield force	$F_y = K_1 D_y$
(4)	Post-yield stiffness to pre-yield stiffness ratio	$\alpha = K_2 / K_1$

Table 2 Relationships between the main mechanical parameters of the semi-active devices

Equation	Mechanical parameter	Formulation
(5)	Control force	$\dot{f}_d = -\frac{k_d}{c_d(u)} f_d + k_d \dot{z}_d$
(6)	Controllable device damping	$c_d(u) = c_{min}(1-u) + c_{max}u$
(7)	Control rule	$u = H(f_d \cdot V_a)$

Relationships between the main mechanical parameters of the semi-active devices are listed in Table 2. The control force (f_d) of the Maxwell element can be calculated via Eq. (5) depending on the controllable damping ($c_d(u)$), the stiffness of the device (k_d), and the relative velocity across the device ($\dot{z}_d$). As shown in Eq. (6), the controllable damping ($c_d(u)$) depends on the control signal u, where, c_{max} and c_{min} are the maximum and the minimum damping, respectively. The optimum value of the controllable damping can be obtained according to the change of the control signal that is dependent on the control rule. In this study, the semi-active control device is modeled using the bang-bang pseudo-skyhook control rule (Karnopp *et al.* 1974) given in Eq. (7), where H(.) and V_a are the Heaviside step function and the absolute velocity, respectively. The control rule ensures optimal damping by turning the valve on and off. If $f_d.V_a \leq 0$, the damping is minimized by turning the damper off (u=0). Conversely, the control signal u decides to turn the damper on (u=1) if $f_d.V_a > 0$ and thus the damping is maximized.

The actual values of the mechanical parameters of the semi-active isolation elements may be different from the design values due to the variations in the material properties, element dimensions, production method, errors in assembly, etc. In addition, it has been emphasized by (Cheng *et al.* 2008) that the characteristic parameters of the isolation system components may also change due to the effects such as contamination, aging and temperature. The mechanical parameters of the semi-active isolation system listed in Tables 1 and 2 are to be considered as random variables to take such potential uncertainties into account in the context of a probabilistic analyses.

2.3 DBASIS-SA -MC

3DBASIS (Nagarajaiah *et al.* 1991) is a software widely used in the academic field for performing linear and nonlinear time-history analysis of three dimensional base

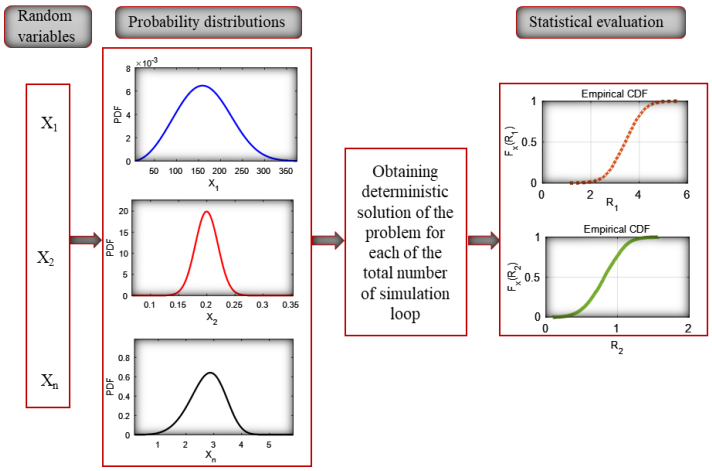

Fig. 1 Schematic illustration of Monte-Carlo Simulation procedure (adapted from Sinha *et al.* 2013).

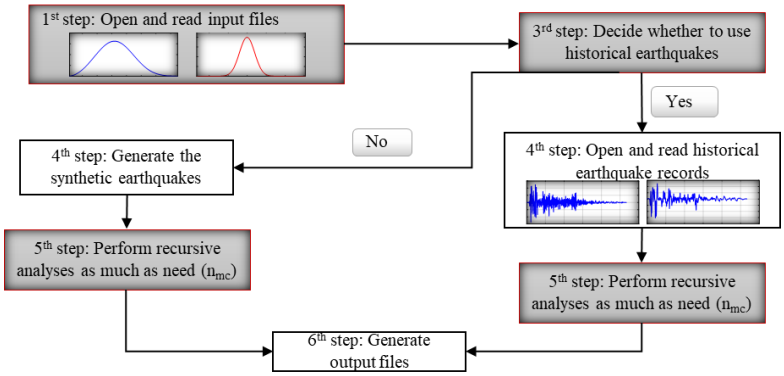

Fig. 2 General flow chart of 3DBASIS-SA-MC program

isolated structures. 3DBASIS program was previously modified by (Gavin *et al.* 2003) to obtain 3DBASIS-SA,which is capable of carrying out bi-directional seismic analyses of three dimensional semi-active isolated buildings.

3DBASIS-SA program is further modified by (Ö ncü-Davas 2018) for conducting recursive analyses (3DBASIS-SA-MC) in order to perform Monte-Carlo Simulations of the semi-active isolated buildings. General flow chart of 3DBASIS-SA-MC program is given in Fig. 2. Firstly, three input files are opened and read in the program: (i) the input file used for modeling of the semi-active isolated building, (ii) the input file containing random variables of the semi-active isolation system, (iii) the input file containing historical earthquake records or random variables used in modeling synthetic near-fault earthquakes -if required-. The modified program is capable of performing the analyses both under historical earthquakes and under synthetic earthquakes. For conducting Monte-Carlo Simulations under historical earthquakes, the program reads the acceleration and velocity records of the ground motions and conducts nonlinear time history analyses as much as the number of MC. Please note that the velocity record of the ground motion is necessary for performing the analyses of semi-active isolated buildings.

3. Benchmark buildings

3-story and 9-story seismically isolated benchmark buildings equipped with semi-active devices used in this study are composed of two main parts as seen in Fig. 3: (1) superstructure which is modeled as 3-dimensional shear building and (2) semi-active isolation system which consists of rubber bearings and semi-active control devices.

3.1 Superstructure

The superstructure plan is symmetric and the floor stiffness is chosen to be the same. The floor masses are assumed to be equal and lumped each floor level. The floor masses and floor stories are adjusted to provide first-mode fixed-base periods of 0.34 s and 0.91 s for the 3-story and 9 story model, respectively. The superstructure modal damping ratios have been set at 5% for all modes in each mode.

3.2 Semi-active isolation system

The semi-active isolation system consists of a total of 25 lead rubber bearings under each column and 8 semi-active control devices placed perpendicularly at each corner of the isolation system (Fig. 3). The detail of a typical corner of the semi-active isolation system is given in Fig. 4.

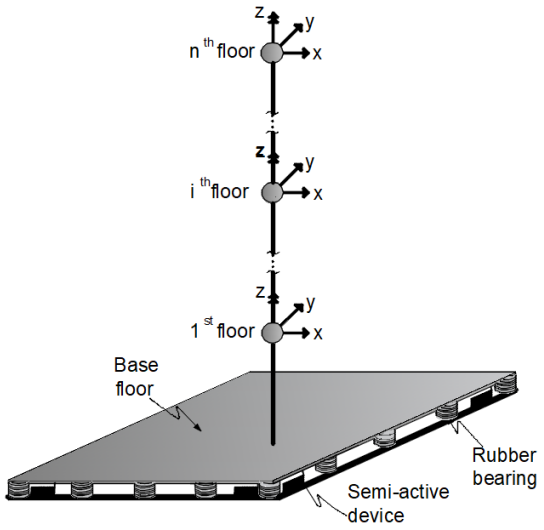

Fig. 3 Schematic representation of the semi-active isolated building model (n=3 for 3-story and n=9 for 9-story model)

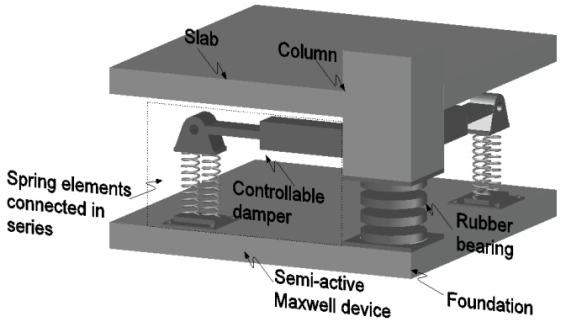

Fig. 4 The detail of a typical corner of the semi-active isolation system

3.2.1. Semi-active maxwell element

For a more realistic investigation considering the probable uncertainties in the characteristic mechanical parameters of the semi-active control device, the device stiffness (k_d), the maximum damping (c_{max}), and the minimum damping (c_{min}) are considered as random variables following normal distribution. Once the random variables for the semi-active devices (i.e., k_d, c_{max}, and c_{min}) are generated, other variables dependent on these ones are calculated via Eqs. (5)-(7).

In this study, the nominal the stiffness of the device (k_d) of the 3 and 9-story buildings are taken as 1250 kN/m and 2500 kN/m, respectively. The nominal value of the maximum damping (c_{max}) is 150 kNs/m and 300 kNs/m for the 3-story and 9-story buildings, respectively. Likely, the nominal value of the minimum damping (c_{min}) are 30 kNs/m and 50 kNs/m for both of them, respectively. The mean values of the random variables are equal to the nominal values and the coefficient of variation (c.o.v.) for the random variables of the semi-active devices is taken as 10%, which is a typical value for most engineering system parameters.

3.2.2 Lead rubber bearings

Here, the post-yield to pre-yield stiffness ratio (α), the yield displacement (D_y), and the yield force (F_y) are considered as random variables, which are among the mechanical properties of the rubber isolators (see Table 1). Then, other variables dependent on these ones (i.e., K_1, K_2, and Q) are calculated via Eqs. (2)-(4). The total weight (W) of 3-story and 9-story benchmark buildings are 12557 kN and 31392 kN, respectively. The nominal values of the isolation period (T_0), the total yield strength ratio (Q/W) and the yield displacement (D_y), which are the main parameters of the isolation system, are considered as 4s, 10% and 20 mm for both buildings, respectively as representative values for a typical practical application. Then, the nominal total post-yield stiffness (K_{2t}) for both buildings are obtained for the assumed nominal isolation period. To obtain the nominal post-yield stiffness for each individual isolators (K_2), the nominal total post-yield stiffness (K_{2t}) is divided by the total number of isolators, i.e. 25. Considering that the total characteristic strength to be equal to 0.10W, the nominal pre-yield stiffness (K_1) is calculated by Eq. (2). Then, the nominal yield strength (F_y) and the nominal post-yield to pre-yield stiffness ratio (α) can be obtained through the relationships given in Eqs. (3) and (4), respectively. Accordingly, the nominal value of the yield force, F_y of the 3 and 9-story buildings are obtained as 52.8 kN and 131.9 kN, respectively. Also, the nominal value of α is calculated as 0.048 for each building. The random variables relating the rubber bearings are assumed to follow a normal distribution with the mean values being equal to the aforementioned nominal values and a 10% coefficient of variation (c.o.v.).

4. Historical pulse-like near-fault earthquakes

Near-fault pulse-like earthquakes attract intense interest from seismologists and engineers as they can cause major structural damage in regions that are close to the seismic source. Near-fault earthquakes are recognized by velocity records containing long-period and large-amplitude velocity pulses (Masaeli *et al.* 2014). Cox and Ashford (2002) explained that the near-fault ground motions are typically observed in distances within 10.0 km from the fault. (Dicleli and Buddaram 2007) used in their study earthquakes recorded within 12.7 km distance to the fault with moment magnitudes greater than 6.7 and maximum pulse velocities greater than 39.1 cm/s as representative near-fault earthquake records. And the Uniform Building Code (UBC, 1997) has specified near-source amplification factors that scale up design spectrum for the seismically isolated buildings located at the close vicinity of the fault line (<10 km). In addition, larger amplification factors have been proposed for the seismically isolated buildings located at the immediate vicinity of the fault line (<10 km). Thus, in this study, a total of 30 pulse-like historical near-fault earthquake records recorded within 10 km of the fault are used which are retrieved from PEER Strong Motion Database (2017) and they are divided into two groups depending on their proximity to the fault (r = 0-6 km and r

Table 3 Historical pulse-like near-fault earthquakes

r=0 ile r=6 km						r=6 km ile r=10 km					
Abbrevation	**Earthquake**	**Date**	**M_w**	**r (km)**	**T_p (s)**	**Abbrevation**	**Earthquake**	**Date**	**M_w**	**r (km)**	**T_p (s)**
TCU065	Chi-Chi Taiwan	1999	7.6	0.6	5.7	CHY024	Chi-Chi Taiwan	1999	7.6	9.6	6.7
TCU068	Chi-Chi Taiwan	1999	7.6	0.3	12.3	SPV	Northridge	1994	6.7	8.4	0.9
YPT	Kocaeli	1999	7.5	4.8	4.9	NWH	Northridge	1994	6.7	5.9	1.4
BPTS	Superstition Hills-02	1987	6.5	1	2.4	LDM	Northridge	1994	6.7	5.9	1.6
HE05	Imperial Valley	1979	6.5	4	4.1	HECC	Imperial Valley	1979	6.5	7.3	4.4
TAZ	Kobe	1995	6.9	0.3	1.8	HE04	Imperial Valley	1979	6.5	7.1	4.8
HE06	Imperial Valley	1979	6.5	1.4	3.7	HE10	Imperial Valley	1979	6.5	8.6	4.5
HE07	Imperial Valley	1979	6.5	0.6	4.4	PUL	Northridge	1994	6.7	7	0.8
LCN	Landers	1992	7.3	2.2	5.1	WVC	Loma Prieta	1989	6.9	9.3	5.6
TAB	Tabas	1978	7.4	2.1	6.2	HHVP	Imperial Valley	1979	6.5	7.5	4.8
WPI	Northridge	1994	6.7	5.5	3	PET	Cape Mendocino	1992	7	8.2	3
JEN	Northridge	1994	6.7	5.4	3.2	LINC	Darfield	2010	7	7.1	7.4
SCE	Northridge	1994	6.7	5.2	3.5	HORC	Darfield	2010	7	7.3	9.9
SYL	Northridge	1994	6.7	5.3	2.4	GRO	Montenegro	1979	7.1	7	1.4
SFERN	San Fernando	1971	6.6	1.8	1.6	TCU063	Chi-Chi Taiwan	1999	7.6	9.8	6.6

= 6-10 km) in order to evaluate the seismic performance of semi-active isolated buildings systematically considering their location with respect to the fault line. The moment magnitudes of earthquakes (M_w) which are selected to be greater than 6.5, the pulse periods (T_p), and the closest fault distances (r) are listed in Table 3. Other details such as peak ground acceleration (PGA), peak ground velocity (PGV) and peak ground displacement (PGD) are presented in Table 4.

5. Results

In order to evaluate the probabilistic behavior of the 3-story and 9-story benchmark semi-active isolated buildings, Monte-Carlo Simulations have been conducted under 30 historical pulse-like earthquakes. The number of Monte-Carlo Simulations for each earthquake is n_{mc}=3,000, which required a total of 180,000 bi-directional non-linear time-history analyses to be carried out. The results are presented in the form of cumulative distribution function (CDF) and probability of failure (P_f) plots for each response parameter, i.e., peak floor accelerations, peak base displacement and peak inter-story drift ratios and they are assessed comparatively with respect to different performance limit thresholds.

5.1 Tolerable limits

The probability of failure (P_f) associated with a particular structural response parameter can be obtained with limit state functions that depend on limit state thresholds. The probability of failure (P_f) can be described as

$$P_f = \frac{n_f}{n_{mc}} \quad (8)$$

Here, n_{mc} is the total number of Monte Carlo simulations and n_f is the number of simulations where the limit state functions g(X) is equal to or less than 0 ($g(X) \leq 0$) which indicates failure. In this study, the limit state functions are formed as

$$g(X) = \text{Limit State Value} - \text{Peak Response} \quad (9)$$

Therefore, the limit state values that correspond to the desired performance limits for the semi-active isolated buildings need to be identified first. In this study, three seismic response parameters are evaluated: (i) Peak floor acceleration which may be directly related to the safety of the vibration-sensitive equipment housed in the building (Ferritto 1984, Alhan and Sahin 2011). Peak floor accelerations can cause more than 80% of non-structural damages (FEMA-NIBS, 2003), (ii) Peak inter-story drift ratio which is directly related to the safety of structural and non-structural elements such as partition walls and windows (Karavasilis and Seo 2011). According to FEMA-NIBS (2003), excessive inter-story drifts lead to the most structural losses; (iii) Peak base displacement which is directly related to the safety of the isolation system (Jangid 2007) and thus the overall safety of the building. Tolerable limit values of peak floor accelerations and peak base displacements for different performance targets have been previously defined in a study by Alhan and Oncu-Davas (2016). Also, in a study evaluating the seismic fragility of a seismically isolated building (Tajammolian *et al*. 2018), four different damage states (slight, moderate, extensive, collapse) in terms of peak floor accelerations and peak inter-story drifts are considered according to the HAZUS-2003 (FEMA-NIBS, 2003). Here, similar performance limits (i.e., limit state values) are adopted as elaborated next

Table 4 Additional information on the historical near-fault pulse-like earthquakes

	Abbrevation	Earthquake	Station	Component	PGA (g)	PGV (cm/s)	PGD (cm)
r= 0-6 km	TCU065	Chi-Chi Taiwan	TCU065	TCU065-E	0.8	92.1	108.7
	TCU068	Chi-Chi Taiwan	TCU068	TCU068-E	0.5	249.5	297
	YPT	Kocaeli	Yarımca	YPT150	0.3	71.9	47.3
	BPTS	Superstition Hills-02	Parachute Test Site	B-PTS225	0.4	134.2	46.1
	HE05	Imperial Valley	El Centro Array #05	H-E05230	0.4	96.9	75.2
	TAZ	Kobe	Takarazuka	TAZ000	0.7	68.4	26.7
	HE06	Imperial Valley	El Centro Array #06	H-E06230	0.4	113.5	72.9
	HE07	Imperial Valley	El Centro Array #07	H-E07230	0.5	113.1	46.9
	LCN	Landers	Lucerne	LCN260	0.7	133.3	113.9
	TAB	Tabas	Tabas	TAB-T1	0.9	123.3	93.6
	WPI	Northridge	Newhall - W. Pico Canyon Rd.	WPI046	0.4	118.1	42.5
	JEN	Northridge	Jensen Filter Plant	JEN022	0.4	111.4	44.6
	SCE	Northridge	Sylmar - Converter Sta East	SCE011	0.9	120.9	34
	SYL	Northridge	Sylmar - Olive View Med FF	SYL360	0.8	129.3	32.1
	SFERN	San Fernando	Pacoima Dam (upper left abut)	PUL194	1.2	114.4	39
r= 6-10 km	CHY024	Chi-Chi Taiwan	CHY024	CHY024-E	0.28	51.1	53.7
	SPV	Northridge	LA-Sepulveda VA Hospital	SPV270	0.75	77.6	11.8
	NWH	Northridge	Newhall - Fire Sta	NWH360	0.59	96.54	34.32
	LDM	Northridge	LA Dam	LDM064	0.43	74.8	19.1
	HECC	Imperial Valley	EC County Center FF	H-ECC092	0.24	73.35	47.98
	HE04	Imperial Valley	El Centro Array #4	H-E04230	0.37	80.37	74.23
	HE10	Imperial Valley	El Centro Array #10	H-E10320	0.17	50.66	35.38
	PUL	Northridge	Pacoima Dam (upper left)	PUL194	1.29	103.3	22.2
	WVC	Loma Prieta	Saratoga - W Valley Coll.	WVC000	0.33	64.9	37.8
	HHVP	Imperial Valley	Holtville Post Office	H-HVP315	0.22	51.43	35.81
	PET	Cape Mendocino	Petrolia	PET090	0.66	88.47	33.2
	LINC	Darfield, New Zeland	LINC	LINCN23E	0.46	108.7	66.6
	HORC	Darfield, New Zeland	HORC	HORCN18E	0.45	105.9	52.9
	GRO	Montenegro, Yugoslavia	GRO	BSO090	0.37	52.8	16.0
	TCU063	Chi-Chi Taiwan	TCU063	TCU063-N	0.13	82.8	52.7

and the results obtained from probabilistic analyses are comparatively evaluated under these limits: It is stated by Pan *et al.* (2005) that the peak displacements of the rubber isolators can range from 40 cm to 100 cm. Therefore, three levels of performance limits for the peak base displacements are selected as Ld_1=40 cm, Ld_2=70 cm and Ld_3=100 cm. The vibration-sensitive equipment housed inside the buildings can be protected and may even be operated during an earthquake if the equipment exposed to the horizontal accelerations does not exceed 10 m/s^2 and 2.5 m/s^2, respectively according to (Worksafe 2011). Thus, three levels of the limit state thresholds for the peak floor accelerations are set as La_1=3 m/s^2, La_2=5 m/s^2 and La_3=10 m/s^2. While the exceedance of the inter-story drift ratio limit of 0.01 may represent the plastic behavior of the superstructure, the limit of 0.005 corresponds to the elastic behavior. Furthermore, when it is desired that non-structural brittle elements are not damaged, the limit of 0.0025 can be taken into account. As a result, the inter-story drift ratio thresholds for three different levels in this study are selected as Ldr_1=0.0025, Ldr_2=0.005 and Ldr_3=0.01. The aforementioned performance limits represent targets varying from the most challenging to the least challenging.

5.2 Fragility curves

The fragility curve or the cumulative density function (CDF) plots are developed for the aforementioned structural responses via Monte-Carlo Simulations. These plots can be used to determine any reliability level, since they give comprehensive information about the probability of exceedance corresponding to any selected limit state value (i.e., performance limit). The curves for peak top floor acceleration (ptfa), peak base displacement (pbd), and peak interstory drift ratios (pdr) corresponding to the historical pulse-like ground motions that are recorded at the

Tablo 5 Statistical results*

		r=0-6 km earthquakes			r=6-10 km earthquakes		
		min	max	mean (at 50% realibility level)	min	max	mean (at 50% realibility level)
3-story	ptfa (m/s^2)	1.53	3.19	2.18	1.14	2.52	1.76
	pdr (-)	$0.8x10^{-3}$	$1.8x10^{-3}$	$1.2x10^{-3}$	$0.66x10^{-3}$	$1.3x10^{-3}$	$0.9x10^{-3}$
	pbd (cm)	16.6	80.5	39.6	8.7	36.9	20.6
9-story	ptfa (m/s^2)	2.45	7.48	4.31	1.72	5.67	3.31
	pdr (-)	$2.3x10^{-3}$	$3.5x10^{-3}$	$5.7x10^{-3}$	$2x10^{-3}$	$4x10^{-3}$	$2.6x10^{-3}$
	pbd (m)	18.9	111	42.7	11	37.6	20.9

*See Figs. 5-7 for visual descriptions of min, max and mean at 50% reliability level

immediate vicinity of the fault line (r= 0-6 km) and at the close vicinity of the fault line (r= 6-10 km) are depicted in Figs. 5-7. The curves that correspond to mean values are also presented on these CDF plots. The probable minimum and maximum values among all earthquakes and the mean values at the 50% reliability level are also extracted from these plots and summarized in Table 5.

The fragility curves in terms of ptfa values are given in Fig. 5 for earthquakes recorded at r= 0-6 km and r= 6 km10 km, separately for 3 and 9-story buildings. As shown in these plots and as presented in Table 5, ptfa values of the buildings with rigid superstructure (3-story) vary from 1.53 m/s^2 to 3.19 m/s^2 under earthquakes within r= 0-6 km, while they attain lower values from 1.14 m/s^2 to 2.52 m/s^2, in case of earthquakes within r=6-10 km. Furthermore, the fragility curves are shifted on the horizontal axis to the right considerably with the increase of the superstructure flexibility (9-story building, Figs. 5(b) and 5(d)). In case of earthquakes at the immediate vicinity of the fault line (r= 0-6 km), the ptfa values of semi-active isolated buildings with flexible superstructures (9-story) attain the largest values which vary from 2.45 m/s^2 to 7.48 m/s^2, much higher compared to the rigid superstructure (3-story) case. The mean values at 50% reliability level also significantly increase from 2.18 m/s^2 to 4.31 m/s^2 (r= 0-6 km) and from 1.76 m/s^2 to 3.31 m/s^2 (r= 6-10 km) as the superstructure flexibility increase (from 3-story to 9-story). Another observation is that the steepness of the fragility (CDF) curves obtained for each earthquake is different. It should be noted at this point that the steepness of the fragility curves indicates how important the effect of the uncertainties in the semi-active isolation system is on the structural response variation. For example, the ptfa fragility curve under TAZ earthquake is steeper than the curve obtained for TAB earthquake (Fig. 5(b)). This shows that the effect of the uncertainties in the semi-active isolation system on ptfa values in case of TAZ earthquake is more limited than TAB earthquake case. Please note that, the maximum value of 5.20 m/s^2 is 10% greater than the minimum value of 4.74 m/s^2 under TAZ earthquake while the maximum ptfa value of 6.33 m/s^2 is 18% greater than minimum ptfa value of 5.37 m/s^2 under TAB earthquake, showing that a higher response variability is observed for TAB earthquake that arise from uncertainties in the isolation system mechanical properties. When the mean CDF curves are examined, it is observed that they are almost straight lines (very small variation) showing that, the influence of semi-active isolation system uncertainty is small when mean values are considered. On the other hand, considering that the CDF curves with the smallest and largest values (i.e., CDF curves for YPT and TCU068 earthquakes) are apart from each other, it can be said that the uncertainties in earthquake loading is more influential on the variation of structural response than the uncertainties in the semi-active isolation system.

Fig. 6 depicts the fragility curves in terms of peak inter-story drift ratios (pdr) for buildings with both rigid and flexible superstructures (i.e., 3-story and 9-story) considering earthquakes recorded both at r= 0-6 km and r=6 km-10 km. As seen from these plots and in Table 5, the pdr values of the 3-story buildings vary from $0.8x10^{-3}$ to $1.8x10^{-3}$ under earthquakes within r=0-6 km (Fig. 6(a)), while they attain lower values, i.e., between $0.66x10^{-3}$ and $1.3x10^{-3}$, in case of earthquakes within r=6-10 km (Fig. 6 (c)). Similar to the general trends of the ptfa, significant increases in the pdr values are observed for the earthquakes at all distances due to the increase of the superstructure flexibility (9-story building, Figs. 6(b) and 6(d)). The pdr values for 9-story building vary between $2.3x10^{-3}$ and 3.5x10-3 for the earthquakes recorded at the immediate vicinity of the fault line (r= 0-6 km) which are much larger than those for 3-story building. As seen from Table 5, the mean pdr values also increase from $1.2x10^{-3}$ to $5.7x10^{-3}$ for r= 0-6 km and from $0.9x10^{-3}$ to $2.6x10^{-3}$ for r= 6-10 km as the superstructure flexibility increases (from 3-story to 9-story).

The fragility curves of the peak base displacements (pbd) for both semi-active isolated buildings (3-story and 9-story) are shown in Figs.7 (a)-7(d) for the earthquakes that are recorded at r= 0-6 km and r= 6-10 km, respectively. Considering the steepness and the scattering (different CDFs for different earthquake records) of the pbd fragility curves, in general it can be stated that the effect of the uncertainties in the semi-active isolation system is less influential on the response variability compared to the variation in earthquake records. Previous deterministic studies in the literature (Kulkarni and Jangid 2003, Alhan and Sahin 2011) have indicated that the influence of the superstructure flexibility on peak base displacements are limited (about 10-15%). However, it is shown in this

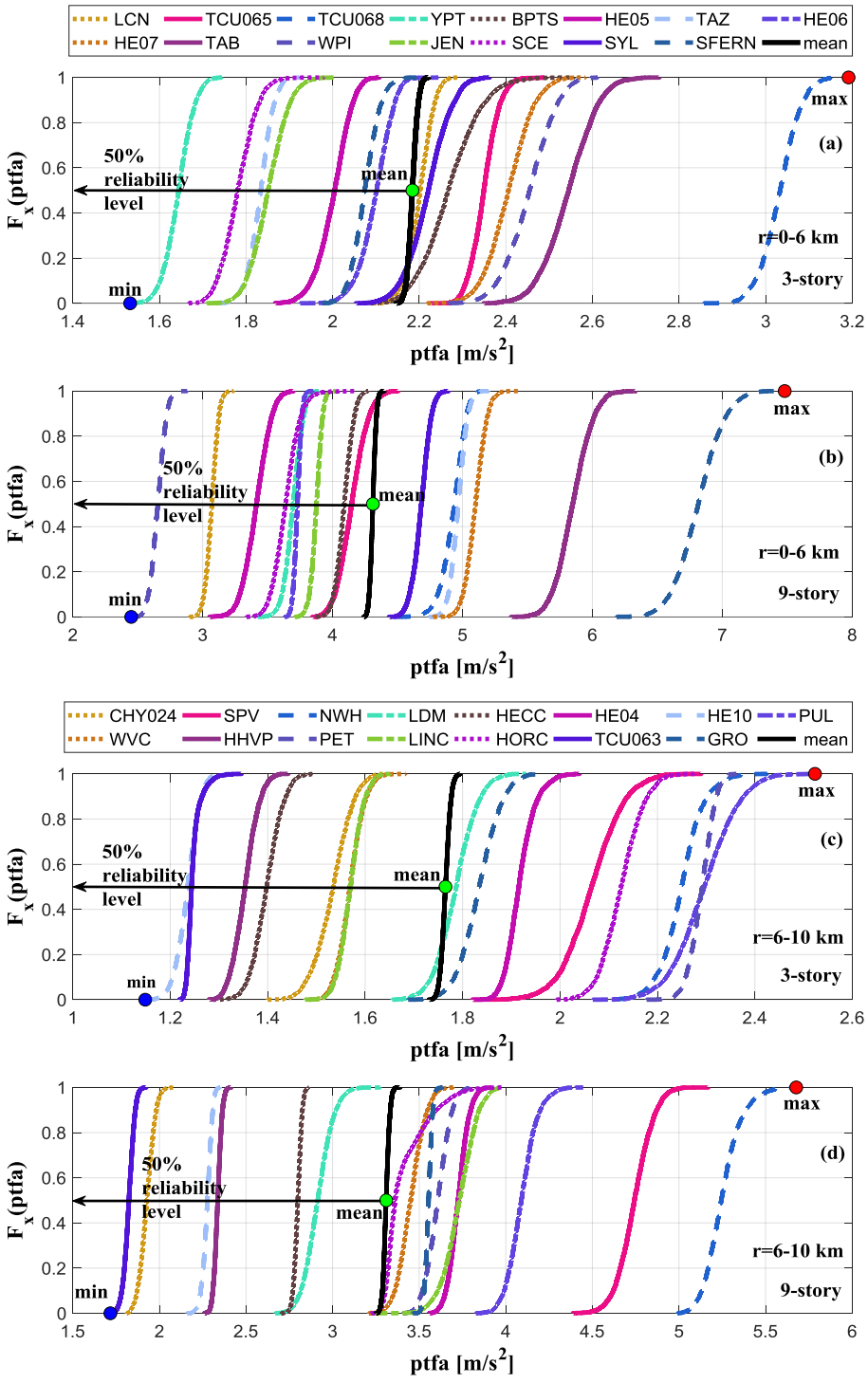

Fig. 5 Fragility curves of the peak top floor accelerations (a)-(b): r=0-6 km, (c)-(d): r=6-10 km

probabilistic study, that the peak base displacement may be considerably affected by the superstructure flexibility when the uncertainties in the isolation system is also taken into account. As an example, for the case of TCU068 earthquake, Figs. 7(a) and 7(b) show that the pbd values of the 3-story building vary between 0.68 m and 0.8 m, whereas the pbd values of the 9-story building for the same record are about 40% higher as they range from 0.95 m to 1.1 m. Another observation is that the peak base displacement values clearly decrease with increasing

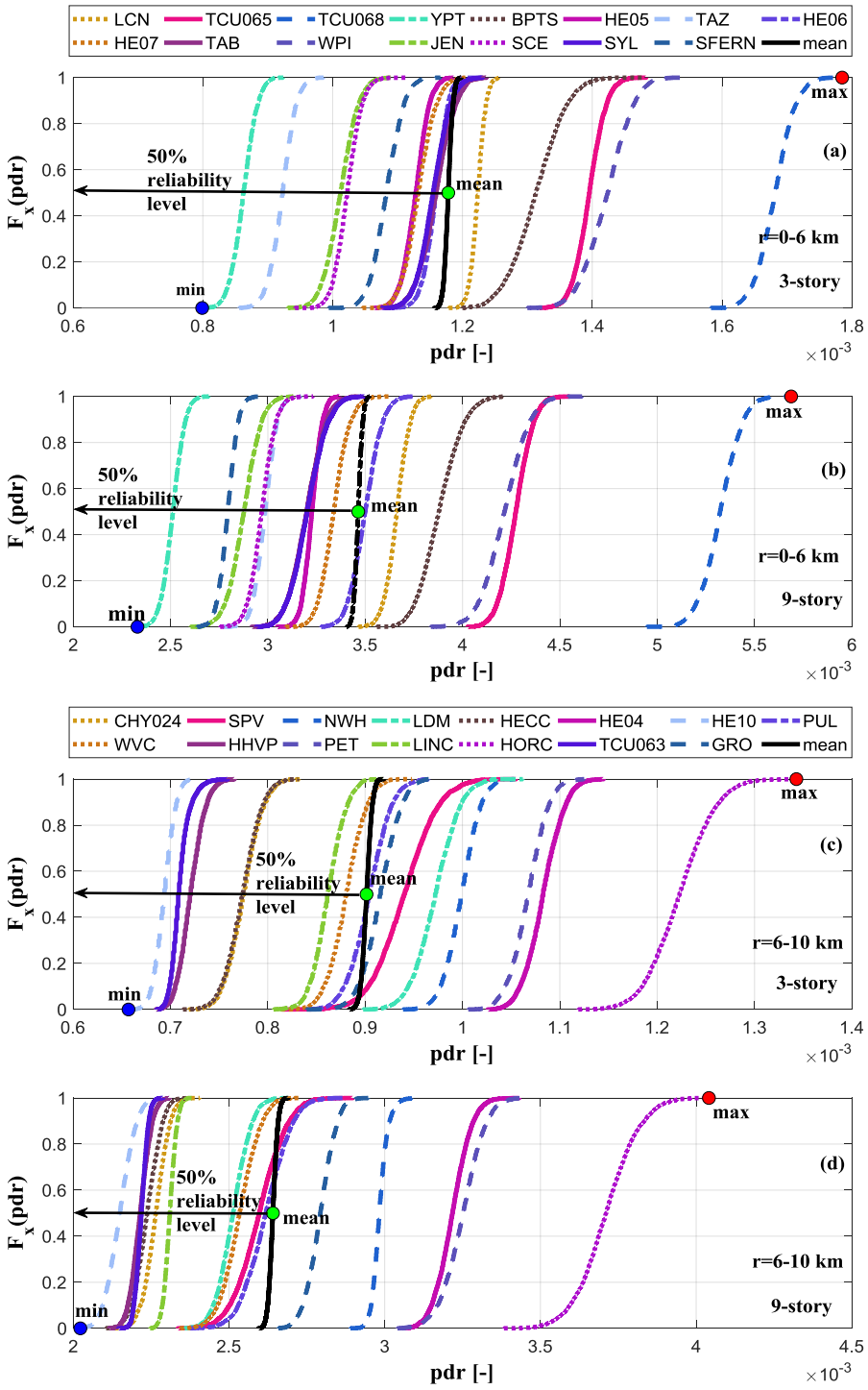

Fig. 6 Fragility curves of the peak inter-story drift ratios (a)-(b): r=0-6 km, (c)-(d): r=6-10 km

distance to the fault (Figs. 7 (c) and 7(d)). For example, the maximum pbd value of the building with rigid superstructure (3-story) is 0.81 m for r=0-6 km earthquakes, while it is merely 0.37 m in case of earthquakes within r=6-10 km (see Table 5). Besides, considering the mean CDF curves for each building (3-story and 9-story, Fig. 7), it is seen that the values are approximately equal to 0.4 m for earthquakes at the immediate vicinity of the fault line (r=0-6 km), while it is reduced by half (to 0.2 m) for earthquakes at the close vicinity of the fault line (r=6-10 km).

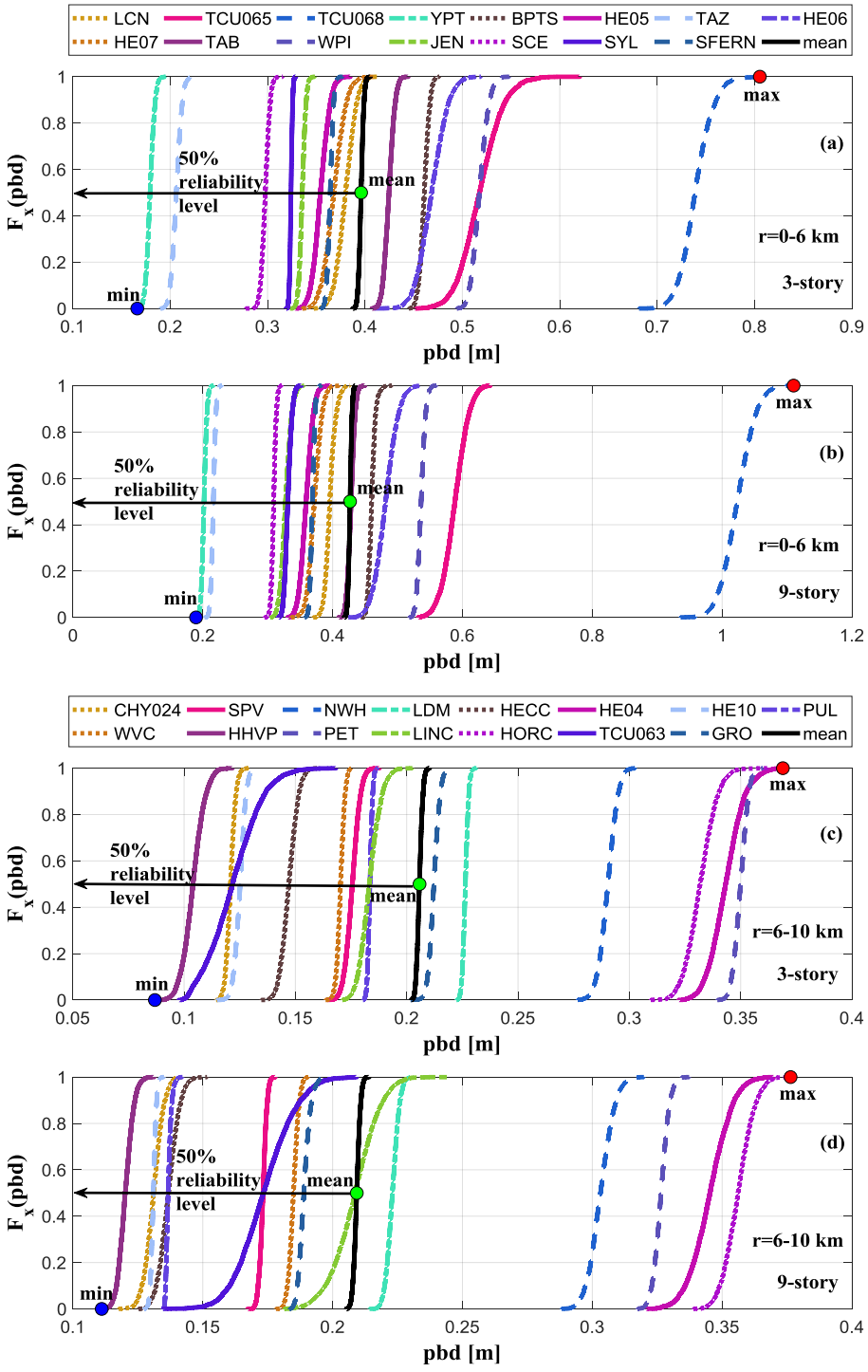

Fig. 7 Fragility curves of the peak base displacements (a)-(b): r=0-6 km, (c)-(d): r=6-10 km

5.3 Probability of failure plots

The probabilities of failure (see Section 5.1 for definition of P_f) in terms of peak floor accelerations, peak inter-story drift ratios, and peak base displacement are calculated considering 3 different limit states for each response parameter (i.e., for performance limits of La_1, La_2, La_3, Ldr_1, Ldr_2, Ldr_3, Ld_1, Ld_2, Ld_3) under each earthquake record given in Tables 3 and 4 for each building (i.e., 3 and 9-story). The results are grouped for the fault distances of r=0-6 km and r=6-10 km and the mean P_f values are obtained for each of these groups for comparison purposes.

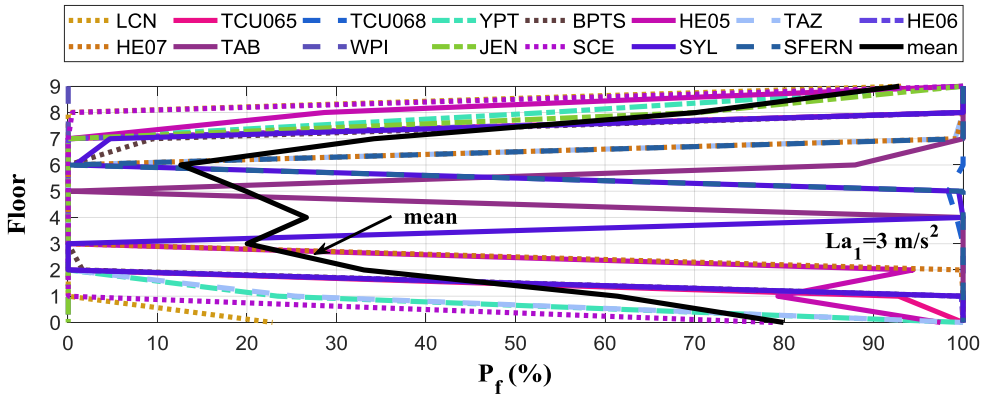

(a)

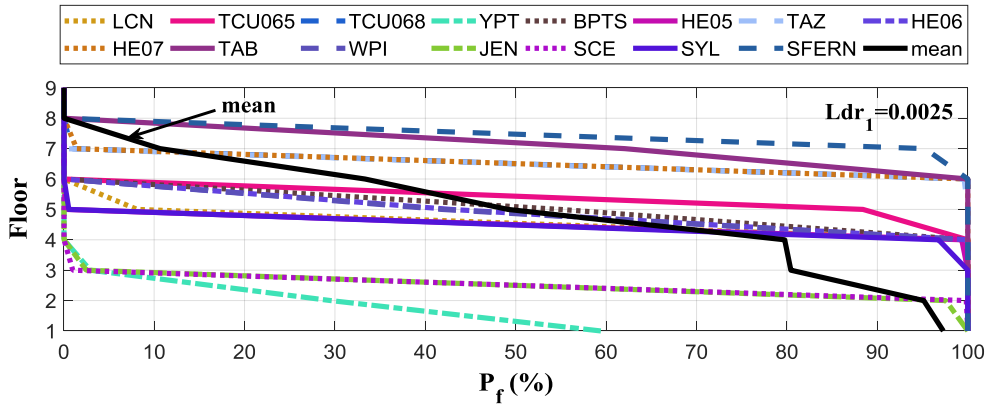

(b)

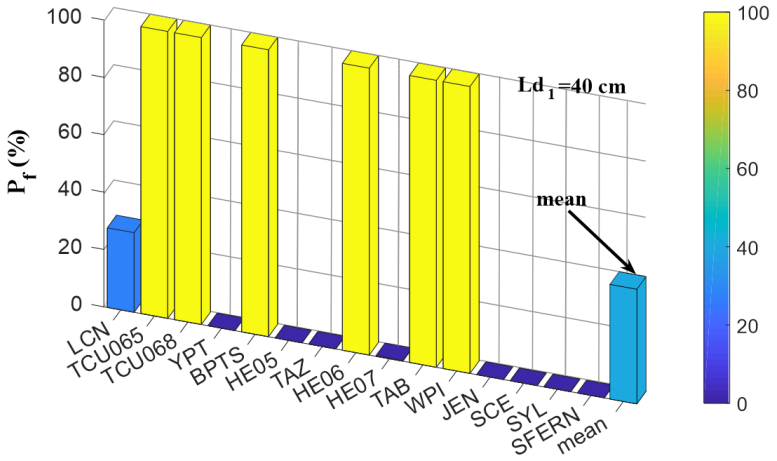

(c)

Fig. 8 Sample probability of failure plots: 9-story buildings at the closest distances to the fault (r=0-6 km) in terms of: (a) peak floor accelerations (0 represents base floor), (b) peak inter-story drift ratios and (c) peak base displacements for the most challenging limits (La_1=3 m/s^2, Ldr_1=0.0025, Ld_1=0.4 m)

Due to the limited space, the probabilities of failure profiles of 9-story building in terms of peak floor accelerations and peak inter-story drift ratios along the height of the building (0 represents base floor) and in terms of peak base displacements are depicted in Fig. 8 under the most challenging limits (La_1, Ldr_1, Ld_1) for the earthquakes within r=0-6 km as representative detailed plots. The mean values of the probabilities of failure are then calculated which are also depicted in these figures. A similar procedure is followed to obtain the mean values of the probabilities of failure for each earthquake group, each building, and each performance limit which are then presented in a comparative manner in Fig. 9.

The mean probabilities of failure in terms of the peak floor accelerations and the peak inter-story drift ratios for all cases are presented in Figs. 9(a), 9(d) and 9(b), 9(c)

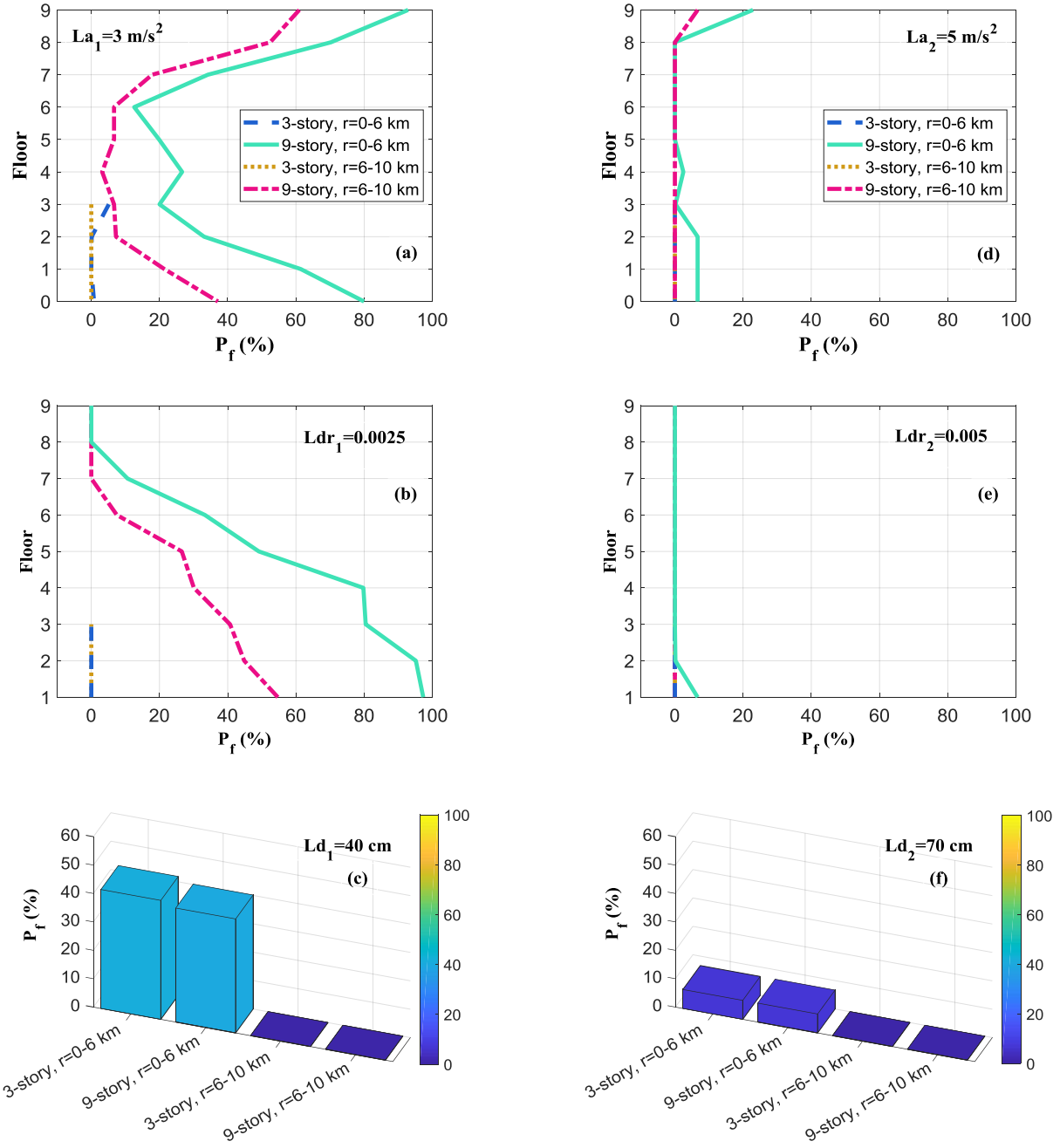

Fig. 9 The mean probability of failures in terms of: (a),(d) peak floor accelerations, (b), (e) peak inter-story drift ratios, (c), (f) peak base displacements under the most challenging and moderate limit thresholds

under the most challenging and the moderate performance limit thresholds along the height of the buildings (0 represents base floor) whereas those relating to the peak base displacements are presented in Figs. 9(c) and 9(f). Since the mean probability of failure values under the least stringent limits (La_3= 10 m/s^2, Ldr_3= 0.01, and Ld_3= 100 cm) is practically P_f=0%, no plots are presented corresponding to these performance limits. Thus, considering that the peak base displacement performance limit of 100 cm is a physically achievable rubber isolator limit and the peak inter-story drift ratio performance limit of 0.01 is a typical seismic code limit, semi-active isolated buildings with both rigid and flexible superstructures without any vibration-sensitive contents (e.g., residential buildings) where peak floor accelerations up to 10 m/s^2 are acceptable can be considered as reliable in the near-fault region (r < 10 km).

Under the most challenging acceleration performance limit (La_1=3 m/s^2, Fig. 9(a)), for 3-story rigid superstructure building, it is seen that P_f=5% only at the top floor for r = 0-6 km, and in other cases P_f is equal to or very close to 0%. On the other hand, the mean P_f values for the flexible superstructure (9-story) are much higher i.e. between 13% and 92% for r=0-6 km earthquakes and 3% to 61% for r=6-

10 km earthquakes. It is also observed that the highest P_f values are obtained at the upper-most floors and the lowest P_f values are obtained at the mid floors. Thus, it would be more preferable to place vibration sensitive equipment at the mid-floors where P_f is lower than the other floors. The mean P_f values are much lower for the moderate acceleration performance limit, La_2=5m/s^2 as seen in Figure 9 (d): P_f=0% for all floors even at the closest distances to the fault (r=0-6 km) for the rigid superstructure (3-story). For flexible superstructure (9-story), P_f=22% even in case of earthquakes at the immediate vicinity of the fault line (r=0-6 km) at the top floor with the values dropping down to P_f=7% in case of earthquakes at the close vicinity of the fault line (r=6-10 km).

The mean probabilities of failure in terms of inter-story drift ratios for 3-story superstructure even under the most challenging performance limit (Ldr_1=0.0025) are equal to P_f=0% at all fault distances (Fig. 8(b)) indicating that brittle non-structural elements in semi-active isolated buildings with rigid superstructures can be effectively protected even at immediate vicinity of the fault line. When P_f profiles are evaluated for 9-story superstructure, P_f=97% is obtained at the lower-most floor which is unacceptably high for Ldr_1=0.0025 in case of r=0-6 km even though it steadily decreases towards upper floors. With the increase in the fault distance (r=6-10 km), the mean P_f values drop significantly where the highest value, P_f =55%, is observed at the lower-most floor. Thus, preservation of brittle non-structural elements of the buildings with flexible superstructures can't be ensured by semi-active isolation particularly at the immediate vicinity of the fault line (r=0-6 km).

As seen in Fig. 9(e), P_f=0% for the rigid superstructure (3-story) semi-active isolated building at all fault distances when the moderate inter-story performance limit (Ldr_2=0.005) is considered. Even for the flexible superstructure (9-story) case, P_f attains a very small value (P_f=5%) in case of earthquakes recorded at immediate vicinity of the fault line (r=0-6 km). And in case of earthquakes recorded at close vicinity of the fault line (r=6-10 km), P_f values for 9-story building drop down to 0%. This indicates that Ldr_2=0.005 can effectively be met and thus semi-active isolated buildings even with flexible superstructures can remain elastic at all fault distances.

When the mean probability of failure values regarding peak base displacements are examined (Figs. 9(c) and 9(f)), it is seen that P_f are almost the same for buildings with both 3-story and 9-story superstructures which shows that the superstructure flexibility does not significantly affect the isolation system reliability of semi-active isolated buildings. For the most challenging base displacement performance limit (Ld_1=40 cm, Fig. 9(c)), it is observed that P_f=40% for both buildings (3-story and 9-story) at immediate vicinity of the fault line (r=0-6 km) which drops down to 0% at the close vicinity of the fault line (r=6-10 km). Considering Ld_1=40 cm corresponding to an economical design, it can be said that this can be fully achieved at the close vicinity of the fault line (r=6-10 km) regardless of the superstructure flexibility while the reliability drops down to 60% at close vicinity of the fault line (r=0-6 km). For the moderate base displacement performance limit (Ld_2=70 cm, Fig. 9(e)) P_f is much smaller (7%) for both superstructures at r=0-6 km, dropping down to 0% at r=6-10 km. As seen, when a moderate base displacement performance limit is considered (by somewhat relaxing economical design requirement), it is possible to ensure a reliable semi-active isolation system.

6. Conclusions

Use of high passive damping may cause amplifications in the floor accelerations and/or inter-story drifts in case of far-fault high-frequency ground excitations. As an alternative for passive systems, semi-active isolation systems can be used to reduce extensive base displacements that can occur in case of near-fault earthquakes without significantly amplifying the floor accelerations and/or inter-story drifts in case of far-fault earthquakes. In this study, the probabilistic behaviour and reliability of semi-active isolated buildings under historical pulse-like earthquakes considering the uncertainties in the semi-active isolation system is investigated in terms of protection of the structural integrity which is governed by base displacement and inter-story drift ratios and the vibration-sensitive equipment which is governed by floor accelerations. Monte-Carlo simulations of both 3-story and 9-story semi-active isolated buildings are performed in order to also assess the influence of the superstructure flexibility on the reliability levels. The results are presented in the form of fragility curves and probability of failure (P_f) profiles. The main outcomes are:

(1) Fragility curves depict that the seismic responses of semi-active isolated buildings notably vary due to the uncertainties in the mechanical parameters of the semi-active isolation system elements and the characteristics of the earthquake excitation. However, the effects of the uncertainties in earthquakes (i.e., record-to-record variability) are much more influential than the uncertainties in the isolation system.

(2) The probabilities of failure of semi-active isolated buildings with flexible superstructures are much higher in terms of floor accelerations and inter-story drift ratios compared to those with rigid superstructures. However, the probability of failures in terms of base displacements is similar for both.

(3) Probabilities of failure in terms of floor accelerations is much lower for semi-active isolated buildings with rigid superstructures compared to those with flexible superstructures. While P_f along the height of rigid superstructures is nearly constant, it varies significantly from floor-to-floor for those with flexible superstructures where they are much lower in mid-floors compared to the lowermost and uppermost floors. These findings indicate that low-rise semi-active isolated buildings would offer more reliable environment for vibration-sensitive equipment and it is advised that the vibration-sensitive equipment be placed on mid-floors of those with flexible superstructures.

(4) Although all ground motion records used in this study

are classified as near-fault earthquakes with fault distances smaller than r=10 km, the probabilities of failure of semi-active isolated buildings located at immediate vicinity of the fault line (r=0-6 km) are significantly higher than those located at close vicinity of the fault line (r=6-10 km).

(5) For immediate vicinity of the fault line (r=0-6 km):

i. Ensuring the reliability of highly vibration-sensitive contents (performance limit 3 m/s^2) housed in semi-active isolated buildings with flexible superstructures can't be possible especially at the upper and lower-most stories. On the other hand, this can be achieved for those with rigid superstructures.

ii. Ensuring the reliability of typical vibration sensitive contents (performance limit 5 m/s^2) housed in semi-active isolated buildings with both rigid and flexible superstructures can be provided.

iii. The inter-story drift performance limit of 0.0025 which represents prevention of damage to brittle non-structural elements (gypsum cracks, window damages, etc.) could be met by the semi-active isolated buildings with rigid superstructures located in near-fault region (r < 10 km) since P_f were obtained as 0% whereas it mostly could not be met by the those with flexible superstructures as P_f were significantly high.

iv. The limit of 0.005, which represents the elastic state of the superstructure, was comfortably met even by those with flexible superstructures as P_f were almost 0%.

v. Peak base displacement limit of 40 cm, representing an economical design, can't be achieved as the reliability level is obtained to be relatively low (60%).

(6) For close vicinity of the fault line (r=6-10 km):

i. Despite increased fault distances, semi-active isolated buildings with flexible superstructures would still have difficulty in providing the reliability for protecting highly vibration-sensitive contents (performance limit 3 m/s^2) particularly at the uppermost and the lowermost floors since average P_f are as high as 60%.

ii. Despite increased fault distances, semi-active isolated buildings with flexible superstructures would still have difficulty in providing the reliability for protecting non-structural brittle elements (performance limit 0.0025 since average P_f are as high as 55%.

iii. Considering 40 cm displacement performance limit corresponding to an economic isolation system design, it can be said that this can be achieved regardless of the superstructure flexibility.

iv. Ensuring the reliability of typical vibration sensitive contents (acceleration performance limit 5 m/s^2) housed in semi-active isolated buildings, prevention of damage to brittle non-structural elements (inter-story drift performance limit 0.0025), and somewhat economic isolation system design (displacement performance limit 70 cm) for both rigid and flexible superstructures can be provided.

(7) Considering 100 cm as a physically achievable isolator limit and 0.01 as a typical seismic code limit for peak inter-story drift ratios, semi-active isolated buildings with both rigid and flexible superstructures without any vibration-sensitive contents, where peak floor accelerations up to 10 m/s^2 are acceptable, can be considered as reliable in the near-fault region (i.e., r < 10 km).

Acknowledgments

The authors would like to thank the Faculty Member Training Program Office (Ö YP) of Istanbul University for providing financial support.

References

Alhan, C. and Gavin, H.P. (2005), "Reliability of base isolation for the protection of critical equipment from earthquake hazards", *Eng. Struct*., **27**(9), 1435-1449.

Alhan, C., Gavin, H.P. and Aldemir, U. (2006), "Optimal control: Basis for performance comparison of passive and semiactive isolation systems", *J. Eng. Mech.- ASCE*, **132**(7), 705-713.

Alhan, C. and Oncu-Davas, S. (2016), "Performance limits of seismically isolated buildings under near-field earthquakes", *Eng. Struct*., **116**, 83-94.

Alhan, C. and Sahin, F. (2011), "Protecting vibration-sensitive contents: an investigation of floor accelerations in seismically isolated buildings", *B Earthq. Eng*., **9**(4), 1203-1226.

Aly, A.M. (2014), "Proposed robust tuned mass damper for response mitigation in buildings exposed to multidirectional wind", *Struct. Des. Tall Spec*., **23**(9), 664-691.

Aly, A.M. and Christenson, R.E. (2008), "On the evaluation of the efficacy of a smart damper: a new equivalent energy-based probabilistic approach", *Smart Mater. Struct*., **17**(4), 045008.

Ayyub, B.M. and Klir, G.J. (2006), Uncertainty modeling and analysis in engineering and the sciences, Chapman and Hall/CRC

Bakhshi, A. and Mostafavi, S. (2014), "Development of fragility curves for base isolated RC structures", *Proceedings of the 9th International Conference on Structural Dynamics*, EURODYN 2014.

Castaldo, P., Amendola, G. and Palazzo, B. (2017), "Seismic fragility and reliability of structures isolated by friction pendulum devices: seismic reliability-based design (SRBD)", *Earthq. Eng. Struct. D*., **46**(3), 425-446.

Chakraborty, S. and Debbarma, R. (2016), "Robust optimum design of tuned liquid column damper in seismic vibration control of structures under uncertain bounded system parameters", *Struct. Infrastruct. E*., **12**(5), 592-602.

Chase, J.G., Barroso, L.R. and Hunt, S. (2004), "The impact of total acceleration control for semi-active earthquake hazard mitigation", *Eng. Struct*., **26**(2), 201-209.

Chaudhuri, A. and Chakraborty, S. (2006), "Reliability of linear structures with parameter uncertainty under non-stationary earthquake", *Struct. Saf*., **28**(3), 231-246.

Cheng, F.Y., Jiang, H. and Lou, K. (2008), Smart structures: innovative systems for seismic response control, CRC Press

Colombo, J.I. and Almazan, J.L. (2015), "Seismic reliability of continuously supported steel wine storage tanks retrofitted with energy dissipation devices", *Eng. Struct.*, **98**, 201-211.

Cox, K.E. and Ashford, S.A. (2002), Characterization for Large Velocity Pulses for Laboratory Testing, Pacific Earthquake Engineering Research Center

Der Kiureghian, A. (2000), "The geometry of random vibrations and solutions by FORM and SORM", *Probabilist. Eng. Mech.*, **15**(1), 81-90.

Dicleli, M. and Buddaram, S. (2007), "Equivalent linear analysis of seismic-isolated bridges subjected to near-fault ground motions with forward rupture directivity effect", *Eng. Struct*., **29**(1), 21-32.

Fallah, A.Y. and Taghikhany, T. (2014), "Robust semi-active control for uncertain structures and smart dampers", *Smart Mater. Struct.*, **23**(9), 095040.

FEMA-NIBS (2003), Multi-Hazard Loss Estimation Methodology, %J Earthquake Model, HAZUS® MH Technical Manual, National Institute of Building Sciences Federal Emergency Management Agency, Washington, DC.

Ferritto, J.M. (1984), "Economics of seismic design for new buildings", *J. Struct. Eng.- ASCE*, **110**(12), 2925-2938.

Gavin, H. and Alhan, C. (2002), "Inter-story drift amplification and damping in passive isolation systems", *Proceedings of the 7th U.S. National Conference on Earthquake Engineering*.

Alhan, C. and Gavin, H. (2004). "A parametric study of linear and non-linear passively damped seismic isolation systems for buildings", Engineering structures, **26(4)**, 485-497.

Gavin, H., Alhan, C. and Oka, N. (2003), "Fault tolerance of semiactive seismic isolation", *J. Struct. Eng. - ASCE*, **129**(7), 922-932.

Gavin, H.P. and Zaicenco, A. (2007), "Performance and reliability of semi-active equipment isolation", *J. Sound Vib.*, **306**(1-2), 74-90.

Gazi, H. and Alhan, C. (2018), "Probabilistic sensitivity of base-isolated buildings to uncertainties", *Smart Struct. Syst.*, **22**(4), 441-457.

Haldar, A. and Mahadevan, S. (2000), Probability, reliability, and statistical methods in engineering design, Wiley New York

Jangid, R.J.E.S. (2007), "Optimum lead–rubber isolation bearings for near-fault motions", *Eng. Struct.*, **29**(10), 2503-2513.

Johnson, E.A., Ramallo, J.C., Spencer Jr, B.F. and Sain, M.K. (1998), "Intelligent base isolation systems", *Proceedings of the Second World Conference on Structural Control*.

Karavasilis, T.L. and Seo, C.Y. (2011), "Seismic structural and non-structural performance evaluation of highly damped self-centering and conventional systems", *Eng. Struct*, **33**(8), 2248-2258.

Karnopp, D., Crosby, M.J. and Harwood, R. (1974), "Vibration control using semi-active force generators", *J. Eng. Industry*, **96**(2), 619-626.

Kulkarni, J.A. and Jangid, R.S. (2003), "Effects of superstructure flexibility on the response of base-isolated structures", *Shock Vib.*, **10**(1), 1-13.

Madden, G.J., Wongprasert, N. and Symans, M.D. (2003), "Analytical and numerical study of a smart sliding base isolation system for seismic protection of buildings", *Comput.-Aided Civ. Inf.*, **18**(1), 19-30.

Masaeli, H., Khoshnoudian, F. and Tehrani, M.H. (2014), "Rocking isolation of nonductile moderately tall buildings subjected to bidirectional near-fault ground motions", *Eng. Struct.*, **80**, 298-315.

Nagarajaiah, S., Reinhorn, A.M. and Constantinou, M.C. (1991), "3D-BASIS-nonlinear dynamic analysis of three-dimensional base isolated structures: Part II".

Öncü-Davas, S. (2018), Probabilistic Behavior of Buildings with Semi-active Seismic Isolation Systems under Earthquake Loads, Istanbul University, PhD Dissertation.

Öncü-Davas, S. and Alhan, C. (2019), "Reliability of semi-active seismic isolation under near-fault earthquakes", *Mech. Syst. Signal Pr.*, **114**, 146-164.

Padmanabhan, D., Agarwal, H., Renaud, J.E. and Batill, S.M. (2006), "A study using Monte Carlo simulation for failure probability calculation in reliability-based optimization", *Optim. Eng.*, **7**(3), 297-316.

Pan, P., Zamfirescu, D., Nakashima, M., Nakayasu, N. and Kashiwa, H. (2005), "Base-isolation design practice in Japan: Introduction to the post-kobe approach", *J. Earthq. Eng.*, **9**(1), 147-171.

Papaioannou, I., Breitung, K. and Straub, D. (2013). "Reliability sensitivity analysis with Monte Carlo methods", ICOSSAR 2013.

PEER (2017), Pacific Earthquake Engineering Research Center, University of California, Berkeley Berkeley, CA

Perotti, F., Domaneschi, M. and De Grandis, S. (2013), "The numerical computation of seismic fragility of base-isolated Nuclear Power Plants buildings", *Nucl. Eng. Des.*, **262**, 189-200.

Pradlwarter, H.J., Schueller, G.I. and Dorka, U. (1998), "Reliability of MDOF-systems with hysteretic devices", *Eng. Struct.*, **20**(8), 685-691.

Providakis, C.P. (2008), "Effect of LRB isolators and supplemental viscous dampers on seismic isolated buildings under near-fault excitations", *Eng. Struct.*, **30**(5), 1187-1198.

Providakis, C.P. (2009), "Effect of supplemental damping on LRB and FPS seismic isolators under near-fault ground motions", *Soil Dynam. Earthq. Eng.*, **29**(1), 80-90.

Roy, B.K., Chakraborty, S. and Mihsra, S.K. (2014), "Robust optimum design of base isolation system in seismic vibration control of structures under uncertain bounded system parameters", *J. Vib. Control*, **20**(5), 786-800.

Saaed, T.E., Nikolakopoulos, G., Jonasson, J.E. and Hedlund, H. (2015), "A state-of-the-art review of structural control systems", J Vib Control, **21(5)**, 919-937.

Saha, S.K., Matsagar, V. and Chakraborty, S. (2016), "Uncertainty quantification and seismic fragility of base-isolated liquid storage tanks using response surface models", *Probabilist. Eng. Mech.*, **43**, 20-35.

Shenton III, H.W. and Holloway, E.S. (2000), "Effect of stiffness variability on the response of isolated structures", *Earthq. Eng. Struct. D.*, **29**(1), 19-36.

Sinha, K.C., Labi, S. and Bai, Q. (2013), "Uncertainties in Transportation Infrastructure Development and Management", *Proceedings of the International Symposium on Engineering under Uncertainty: Safety Assessment and Management (ISEUSAM-2012)*.

Symans, M.D., Madden, G.J. and Wongprasert, N. (2000), "Experimental study of an adaptive base isolation system for buildings", *Proceedings of the 12th World Conf. on Earthquake Eng.*, 12WCEE.

Tajammolian, H., Khoshnoudian, F., Rad, A.R. and Loghman, V. (2018), "Seismic fragility assessment of asymmetric structures supported on TCFP bearings subjected to near-field earthquakes", Structures.

UBC (1997), Uniform Building Code, UBC-97.p

Worksafe (2011), Worksafe Technologies, ISO-Base Seismic Isolation Platform, http://www.worksafetech.com/pages/isotest.html.

YeganehFallah, A. and Attari, N.K.A. (2017), "Robust control of seismically excited cable stayed bridges with MR dampers", *Smart Mater. Struct.*, **26**(3), 035056.

YeganehFallah, A. and Taghikhany, T. (2014), "Robust semi-active control for uncertain structures and smart dampers", *Smart Mater. Struct.*, **23**(9), 095040.

FC